FEBS Letters 489 (2001) 202–207 FEBS 24520

Disulfide bridge reorganization induced by proline mutations in maurotoxin

E. Carlier[a], Z. Fajloun[b], P. Mansuelle[b], M. Fathallah[b], A. Mosbah[c], R. Oughideni[b], G. Sandoz[a], E. Di Luccio[b], S. Geib[a], I. Regaya[b], J. Brocard[a], H. Rochat[b], H. Darbon[c], C. Devaux[b], J.M. Sabatier[b], M. de Waard[a,*]

[a] *Laboratoire de Neurobiologie des Canaux Ioniques, INSERM U464, IFR Jean Roche, Faculté de Médecine Nord, Bd Pierre Dramard, 13916 Marseille Cedex 20, France*
[b] *Laboratoire de Biochimie, CNRS UMR 6560, IFR Jean Roche, Faculté de Médecine Nord, Bd Pierre Dramard, 13916 Marseille Cedex 20, France*
[c] *AFMB, CNRS UPR 9039, IFR1, 31 Chemin Joseph-Aiguier, 13402 Marseille Cedex 20, France*

Received 1 December 2000; accepted 21 December 2000

First published online 18 January 2001

Edited by Pierre Jolles

Abstract Maurotoxin (MTX) is a 34-residue toxin that has been isolated from the venom of the chactidae scorpion *Scorpio maurus* palmatus, and characterized. Together with Pi1 and HsTx1, MTX belongs to a family of short-chain four-disulfide-bridged scorpion toxins acting on potassium channels. However, contrary to other members of this family, MTX exhibits an uncommon disulfide bridge organization of the type C1–C5, C2–C6, C3–C4 and C7–C8, versus C1–C5, C2–C6, C3–C7 and C4–C8 for both Pi1 and HsTx1. Here, we report that the substitution of MTX proline residues located at positions 12 and/or 20, adjacent to C3 (Cys_{13}) and C4 (Cys_{19}), results in conventional Pi1- and HsTx1-like arrangement of the half-cystine pairings. In this case, this novel disulfide bridge arrangement is without obvious incidence on the overall three-dimensional structure of the toxin. Pharmacological assays of this structural analog, [A_{12},A_{20}]MTX, reveal that the blocking activities on *Shaker* B and rat Kv1.2 channels remain potent whereas the peptide becomes inactive on rat Kv1.3. These data indicate, for the first time, that discrete point mutations in MTX can result in a marked reorganization of the half-cystine pairings, accompanied with a novel pharmacological profile for the analog.

Key words: Maurotoxin; Scorpion toxin; Potassium channel; Synthetic peptide; Half-cystine pairing; *Xenopus* oocyte

1. Introduction

Maurotoxin (MTX), a toxin from the venom of the Tunisian chactidae scorpion *Scorpio maurus* palmatus, is a 34-mer peptide cross-linked by four disulfide bridges [1]. MTX belongs to a distinct family of short-chain scorpion toxins with less than 40 residues, that are active on several potassium channel subtypes (Kv and SK channels). Contrary to most short-chain K^+ channel-acting scorpion toxins, this family can be distinguished by the presence of an additional disulfide bridge (four instead of the three commonly present in such toxins). This structural class also includes Pi1 and HsTx1 from the venoms of the scorpions *Pandinus imperator* [2] and *Heterometrus spinnifer* [3], respectively. These toxins share from 53 to 68% sequence identity with MTX but display different pharmacological selectivities. For instance, MTX and Pi1 are both active on apamin-sensitive SK channels, whereas HsTx1 is reportedly inactive on this channel type. Also, MTX was found to be active on rat Kv1.3 channels contrary to synthetic Pi1 [4]. Interestingly, MTX structurally differs from Pi1 and HsTx1, but also from other 'classical' three-disulfide-bridged scorpion toxins, by its unique disulfide bridge pattern. In three-disulfide-bridged toxins, the half-cystine pairings are of the type C1–C4, C2–C5 and C3–C6 (e.g. charybdotoxin, P05, agitoxin 2, leiurotoxin 1). In short-chain four-disulfide-bridged toxins, this pattern is altered by the insertion of two additional half-cystines within the amino acid sequence, one located after C3 and the other after C6. As a result, two novel patterns of the disulfide bridges are experimentally found depending on the toxin: (i) a pattern of the type C1–C5, C2–C6, C3–C7 and C4–C8 in both Pi1 and HsTx1 (which corresponds to an organization similar to that observed in three-disulfide-bridged toxins) and (ii) an uncommon pattern of the type C1–C5, C2–C6, C3–C4 and C7–C8 in MTX. These two patterns possess in common the first two disulfide bridges but differ in the two remaining disulfides. Though differences in pharmacological properties between short-chain four-disulfide-bridged toxins obviously rely on their distinct amino acid sequences, it is also likely that changes in half-cystine pairings may contribute to discrete conformational alterations and repositioning of key residues that are involved in toxin selectivity. In MTX, we noticed that the two proline residues in positions 12 and 20 are adjacent to the non-conventional disulfide bridge C3–C4 (Cys_{13}–Cys_{19}). Though these residues are also present in homologous positions in HsTx1, Pi1 and Pi4, we expected that structural variations induced by the mutagenesis of these proline residues could favor the shift from a MTX-like to a Pi1/HsTx1-like disulfide bridge pattern. To test this hypothesis, we chemically synthesized by the solid-phase method an MTX

*Corresponding author. Fax: (33)-491-09 05 06.
E-mail: dewaard.m@jean-roche.univ-mrs.fr

Abbreviations: HPLC, high-pressure liquid chromatography; MTX, maurotoxin, a scorpion toxin from the venom of *Scorpio maurus* palmatus; Pi1, a scorpion toxin from the venom of *Pandinus imperator*; HsTx1, toxin 1 from the venom of the scorpion *Heterometrus spinnifer*

0014-5793/01/$20.00
PII: S0014-5793(00)02433-9

analog ([A_{12},A_{20}]MTX) in which the two proline residues are substituted by alanine residues. Our data show that these substitutions are responsible for a Pi1- and HsTx1-like rearrangement of the half-cystine pairings of MTX accompanied by subtle changes in pharmacological activity.

2. Materials and methods

2.1. Materials

N-α-fluorenylmethyloxycarbonyl (*N*-α-Fmoc)-L-amino acids, Fmoc-amide resin and reagents used for peptide synthesis were obtained from Perkin-Elmer. Solvents were analytical grade products from SDS. Enzymes (trypsin and chymotrypsin) were obtained from Boehringer Mannheim.

2.2. Chemical synthesis and physicochemical characterization of [A_{12},A_{20}]MTX

[A_{12},A_{20}]MTX was obtained by the solid-phase method [5] using a peptide synthesizer (Model 433A, Applied Biosystems). Peptide chains were assembled stepwise on 0.25 meq of Fmoc-amide resin (0.89 meq of amino group/g) using 1 mmol of Fmoc-amino acid derivatives. *N*-α-amino groups were deprotected by treatment with 18 and 20% (v/v) piperidine/*N*-methylpyrrolidone for 3 and 8 min, respectively. The Fmoc-amino acid derivatives were coupled (20 min) as their hydroxybenzotriazole active esters in *N*-methylpyrrolidone (four-fold excess). The peptide resin (about 2 g) was treated for 2.5 h at room temperature with a mixture of trifluoroacetic acid (TFA)/H_2O/thioanisole/ethanedithiol (88:5:5:2, v/v) in the presence of crystalline phenol (2.25 g). After lyophilization, the crude reduced peptide (2 mM) was oxidized in 200 mM Tris–HCl buffer, pH 8.3. [A_{12},A_{20}]MTX was purified by reversed-phase high-pressure liquid chromatography (HPLC) (Perkin-Elmer, C_{18} Aquapore ODS 20 μm, 250×10 mm) by means of a 60-min linear gradient of 0.08% (v/v) TFA/0–30% acetonitrile in 0.1% (v/v) TFA/H_2O at a flow rate of 6 ml/min ($\lambda = 230$ nm). The homogeneity and identity of [A_{12},A_{20}]MTX was assessed by: (i) analytical C_{18} reversed-phase HPLC (Merck, C_{18} Lichrospher 5 μm, 4×200 mm) using a 60-min linear gradient of 0.08% (v/v) TFA/0–60% acetonitrile in 0.1% (v/v) TFA/H_2O at a flow rate of 1 ml/min; (ii) amino acid analysis after acidolysis (6 N HCl/2% (w/v) phenol, 20 h, 118°C, N_2 atmosphere); and (iii) mass determination by matrix-assisted laser desorption-ionization time-of-flight (MALDI-TOF) mass spectrometry.

2.3. Structural characterization of [A_{12},A_{20}]MTX: assignment of half-cystine pairings by enzyme cleavage and Edman sequencing analysis

[A_{12},A_{20}]MTX (800 μg) was incubated either with a mixture of trypsin and chymotrypsin at 10% (w/w) in 0.2 M Tris–HCl, pH 7.1, for 12 h at 37°C. The peptide fragments were then purified by analytical reversed-phase HPLC (Vydac, C_{18} 5 μm column, 4×150 mm) with a 60-min linear gradient of 0.08% (v/v) TFA/0–60% acetonitrile in 0.1% (v/v) TFA/H_2O at a flow rate of 1 ml/min ($\lambda = 230$ nm). The peptide fragments were hydrolyzed (6 N HCl/phenol) and their amino acid content was analyzed (Beckman, System 6300 amino acid analyzer). The peptides were also characterized by mass spectrometry analysis (RP-DE Voyager, Perseptive Biosystems) and Edman sequencing (Applied Biosystems 470A).

2.4. Conformational analysis of [A_{12},A_{20}]MTX by one-dimensional (1D) nuclear magnetic resonance (NMR)

5 mg of MTX or its structural analog, [A_{12},A_{20}]MTX, were dissolved in 0.5 ml of a mixture of H_2O:D_2O (9:1, v/v). All ^{1}H-NMR measurements were obtained on a Bruker DRX 500 spectrometer equipped with an HCN probe and self-shielded triple axis gradients were used. The experiments were performed at 300 K.

2.5. Molecular modeling

Molecular modeling was performed using MSI InsightII(98) software package on an O2 silicon graphics workstation. We used the Biopolymer module for proline mutations and disulfide bridge reorganization and the Discover program for energy minimization. The molecular mechanics method has been applied with the parameters of the consistent valence force field (CVFF). Starting geometries of MTX and [A_{12},A_{20}]MTX were preliminary minimized by the steepest descent method, then refined by the conjugate gradient method until the final root-mean-square derivative of the energy was less than 0.001 kcal mol^{-1} $Å^{-1}$ in each case.

2.6. Binding assay of [^{125}I]apamin and competition by [A_{12},A_{20}]MTX onto rat brain synaptosomes

Rat brain synaptosomes (P2 fraction) were prepared as described by Gray and Whittaker [6]. The protein content was determined by a modified Lowry method. [^{125}I]apamin (2000 Ci/mmol) was obtained according to Seagar et al. [7]. Aliquots of 50 μl 0.1 nM [^{125}I]apamin were added to 400 μl synaptosome suspension (0.4 mg protein/ml). Samples were incubated for 1 h at 4°C with 50 μl of various concentrations of [A_{12},A_{20}]MTX in 500 μl final volume. The incubation buffer was 25 mM Tris–HCl, 10 mM KCl, pH 7.2. The samples were centrifuged and the resulting pellets were washed three times in 1 ml of the same buffer. Bound radioactivity was determined by γ counting (Packard Crystal II). The values expressed are the means of triplicate experiments ± S.D. Non-specific binding, less than 10% of the total binding, was determined in the presence of an excess (10 nM) of unlabeled apamin.

2.7. Oocyte preparation and electrophysiological recordings

Xenopus laevis oocytes were prepared for cRNA injection and electrophysiological recordings as described [8]. Plasmids coding for K^+ channels were linearized with *Sma*I (*Shaker* B), *Not*I (rat Kv1.1), *Xba*I (rat Kv1.2) and *Eco*RI (rat Kv1.3), and transcribed into cRNA with T7 or SP6 (mMessage mMachine kit, Ambion). The cRNA were stored frozen in H_2O at −80°C at 1 μg/μl. Cells were micro-injected 2 days later with 50 nl of cRNA (0.1–0.2 μg/μl *Shaker* B, rat Kv1.1, rat Kv1.2 or rat Kv1.3 channels) and incubated 2–6 days at 16°C into a defined nutrient oocyte medium [9] before current recordings. Both current and voltage electrodes were filled with 140 mM KCl and had resistances ranging from 0.5 to 1 MΩ. Currents were recorded using a voltage-clamp amplifier (GeneClamp 500, Axon Instruments, Burlingame, CA, USA) interfaced with a 16-bit AD/DA converter (Digidata 1200A, Axon Instruments) for acquisition and voltage protocol application. Voltage pulses were delivered every 15 s from a holding potential of −80 mV. Current signals were captured at 10 kHz and low pass-filtered at 2 kHz using an eight-pole Bessel filter. The extracellular recording solution contained (in mM): 88 NaCl, 10 KCl, 2 $MgCl_2$, 0.5 $CaCl_2$, 0.5 niflumic acid, 5 HEPES, pH 7.4 (NaOH). Leak and capacitive currents were subtracted on-line by a P/4 protocol. Peptide solutions were perfused in the recording chamber at a flow rate of 2 ml/min using a ValveBank4 apparatus (Automate Scientific). 0.1% bovine serum albumin was added to the recording and perfusion solutions to prevent [A_{12},A_{20}]MTX loss to the plastic chamber and tubules. Data analysis was performed using pCLAMP 6.0.3 software (Axon Instruments, Foster City, CA, USA). The results are presented as mean ± S.E.M.

3. Results and discussion

The amino acid sequence of MTX is shown in Fig. 1. The arrangement of half-cystines is of the type C1–C5 (Cys_3–Cys_{24}), C2–C6 (Cys_9–Cys_{29}), C3–C4 (Cys_{13}–Cys_{19}) and C7–C8 (Cys_{31}–Cys_{34}). This disulfide bridge organization is uncommon amongst known scorpion toxins since 'conventional' pairings are either of the type C1–C4, C2–C5 and C3–C6 for three-disulfide-bridged toxins or C1–C5, C2–C6, C3–C7 and C4–C8 for toxins cross-linked by four disulfide bridges (Pi1- and HsTx1-like toxins). The reticulation of MTX is peculiar with regard to the two last disulfide bridges C3–C4 (Cys_{13}–Cys_{19}) and C7–C8 (Cys_{31}–Cys_{34}) since they form cyclic domains with contiguous half-cystines. In MTX, we hypothesized that mutations of both or either one of the two proline residues in positions 12 and 20 may be accompanied by structural variations that could prevent the formation of the C3–C4 disulfide bridge. Pi1 and HsTx1-like half-cystine pairings could result from these mutations in agreement with the fact that Pi7, which lacks one of the homologous proline residue,

presents a bridging that is similar to those of Pi1 and HsTx1 [10]. These proline residues are engaged in *cis* or *trans* -CON- tertiary amide bonds with their preceding amino acid residues instead of forming standard -CONH- peptide bonds. Therefore, we designed and chemically synthesized [A_{12},A_{20}]MTX, a structural analog of the toxin in which prolines were replaced by alanine residues (Fig. 1), and characterized its half-cystine pairings and pharmacology. In case of proline residues playing a pivotal role in the MTX half-cystine pairings, one should expect a reorganization of the disulfide bridges in [A_{12},A_{20}]MTX towards the Pi1/HsTx1 pattern.

Stepwise assembly of [A_{12},A_{20}]MTX was achieved on 0.25 mmol Fmoc-amide resin by means of optimized Fmoc/*t*-butyl chemistry [1,11]. The overall yield of peptide chain assembly was 80%. The profiles of elution by analytical C_{18} reversed-phase HPLC of the crude reduced peptide after final acidolysis is shown in Fig. 2A. The crude peptide was folded/oxidized by 48 h air exposure, and purified to homogeneity by preparative C_{18} reversed-phase HPLC. Mass spectrometry analysis of [A_{12},A_{20}]MTX gave an experimental M_r $(M+H)^+$ of 3561.5, in good agreement with the deduced M_r $(M+H)^+$ of 3561.2 for this analog (Fig. 2B). Amino acid analysis of [A_{12},A_{20}]MTX after acidolysis provides an amino acid content which agreed with the deduced values. To address the pattern of half-cystine connections, [A_{12},A_{20}]MTX was cleaved by a mixture of trypsin and chymotrypsin. An analytical C18 reversed-phase HPLC profile of [A_{12},A_{20}]MTX enzyme digestions shows several proteolytic fragments (Fig. 2C). The peptide fragments were collected, and characterized by means of amino acid analysis, mass spectrometry, and Edman sequencing techniques (Fig. 2D). The half-cystine pairings were unambiguously mapped as Cys3–Cys24 (C1–C5), Cys9–Cys29 (C2–C6), Cys13–Cys31 (C3–C7) and Cys19–Cys34 (C4–C8). This pattern shown in Fig. 2E is of the Pi1/HsTx1 type instead of being of the MTX type. Similarly, we also synthesized and characterized the singly point-mutated analogs, [A12]MTX and [A20]MTX. The results obtained from identical enzyme treatments demonstrate that both peptides folded like [A_{12},A_{20}]MTX, the Pi1/HsTx1-like pattern (data not shown).

This indicates that [A_{12},A_{20}]MTX should be structured according to the common α/β scaffold of scorpion toxins (an α-helix connected by two disulfide bridges to an antiparallel β-sheet structure) since the disulfide bridge arrangement adopted was of the 'conventional' pattern instead of being

MTX

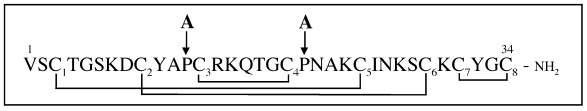

[A_{12},A_{20}]-MTX

Fig. 1. Amino acid sequences, in one-letter code, of natural MTX (top) and its structural analog, [A_{12},A_{20}]MTX (bottom). In the case of MTX, the disulfide bridges are shown in lines [1]. The positions of half-cystines are numbered from 1 to 8.

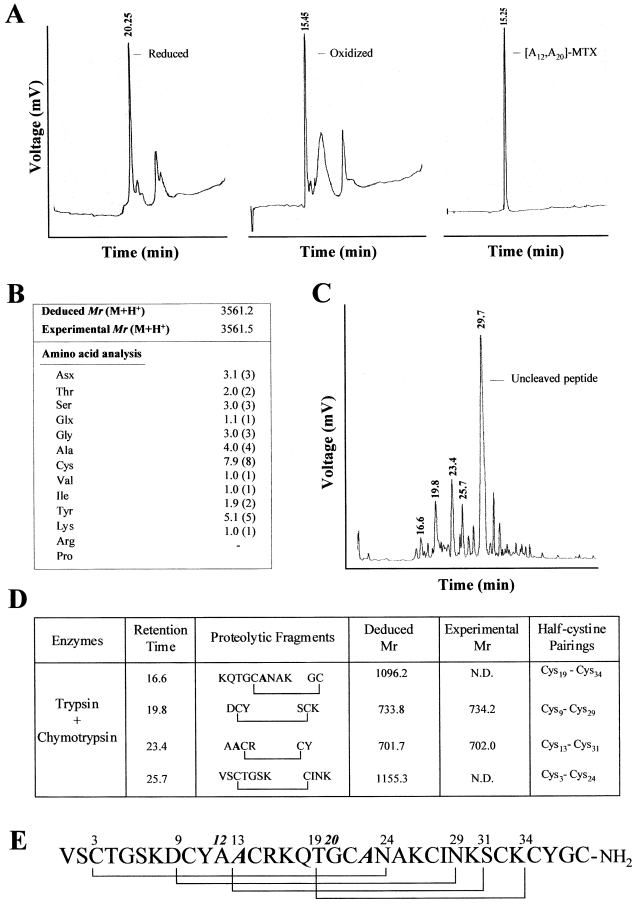

Fig. 2. [A_{12},A_{20}]MTX at different stages of its chemical synthesis and physicochemical characterization. A: Analytical C_{18} reversed-phase HPLC profiles of crude reduced peptide after TFA cleavage (left), crude peptide after folding/oxidation (middle) and purified folded [A_{12},A_{20}]MTX (right). B: The identity of the peptide was confirmed by both MALDI-TOF mass spectrometry analysis and amino acid content determination. C: Analytical C18 reversed-phase HPLC profile of [A_{12},A_{20}]MTX enzyme digestion. The retention times of the uncleaved peptide and proteolytic fragments providing data on the half-cystine pairings are indicated. D: Assignment of the half-cystine pairings by analysis of the peptide fragments obtained by trypsin/chymotrypsin treatment of [A_{12},A_{20}]MTX. After enzyme-based cleavage, the peptide fragments were purified by analytical C18 reversed-phase HPLC and characterized by amino acid analysis, Edman sequencing and mass spectrometry. The peptide sequences deduced from these analyses are shown. Retention times in HPLC, deduced and experimental M_r values of the proteolytic fragments, and established half-cystine pairings are indicated. E: Complete disulfide bridge pattern of synthetic [A_{12},A_{20}]MTX, as experimentally determined by enzyme-based cleavage. The positions of half-cystines residues are indicated by numbers. The disulfide bridges are shown in lines. For conditions, see in Materials and methods.

random. To assess whether proline mutations could be responsible for inducing significant conformational changes in the MTX analog, we performed comparative 1D ^{1}H-NMR analyses of MTX (Fig. 3A, left) and [A_{12},A_{20}]MTX (Fig. 3A, right). In addition, an energy-minimized model of [A_{12},A_{20}]MTX (Fig. 3B, right) has been constructed on the basis of the experimentally mapped disulfide bridges, and compared with the 3D structure of MTX (Fig. 3B, left). Together, the structural data indicate that the overall α/β scaffold of scorpion toxin is maintained in [A_{12},A_{20}]MTX, in

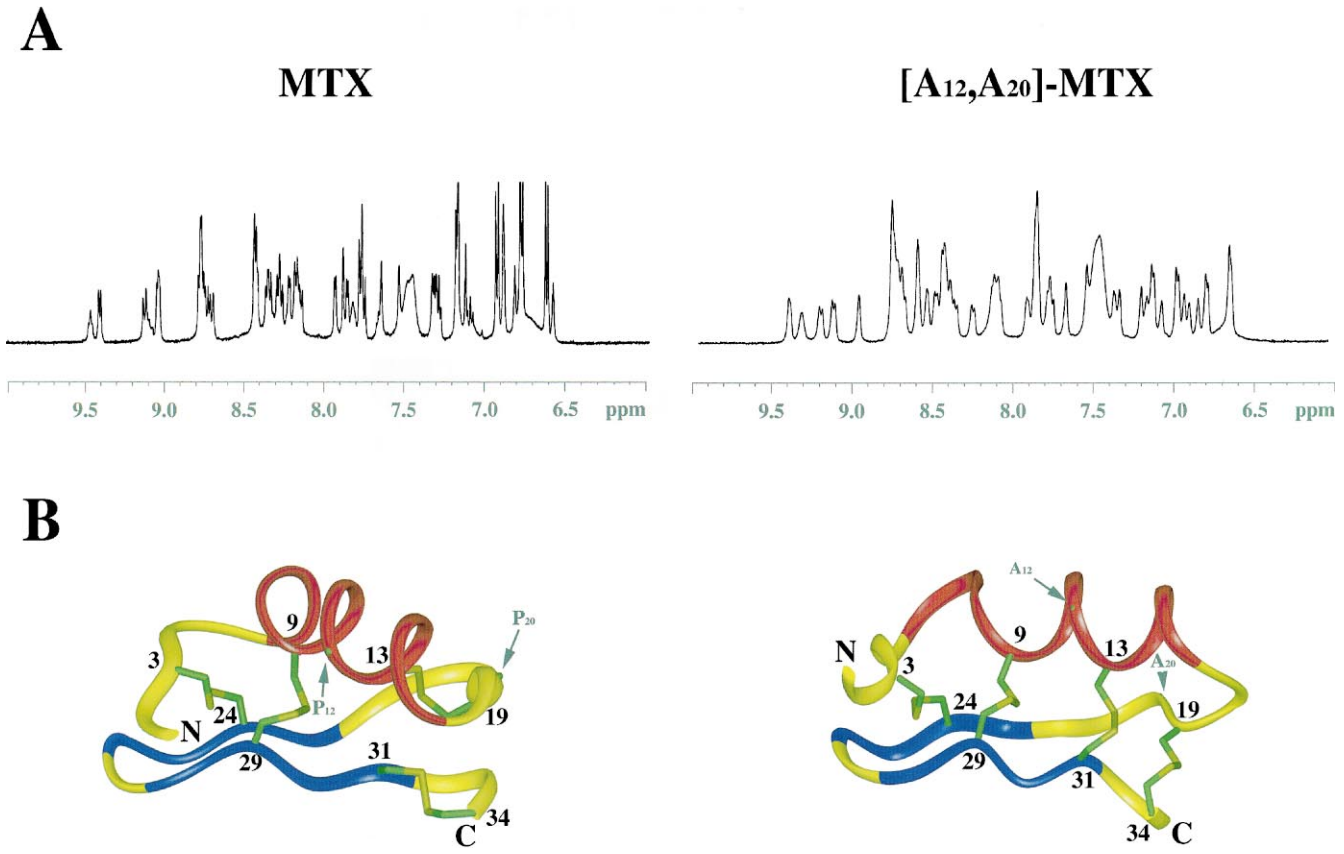

Fig. 3. Conformational analysis of [A_{12},A_{20}]MTX versus MTX. A: 1D NMR spectra of synthetic MTX (left) and its structural analog, [A_{12},A_{20}]MTX (right). For conditions, see Section 2. B: Ribbon representations of the 3D structure in solution of synthetic MTX (left, from the PDB), and the averaged minimized structure of an [A_{12},A_{20}]MTX model (right).

agreement with the concept that this scaffold is not dramatically altered by the two distinct disulfide bridge patterns that are observed in MTX and Pi1/HsTx1. According to the model of [A_{12},A_{20}]MTX, a marked structural difference between MTX and [A_{12},A_{20}]MTX appears to be the relative angle between the axis of the α-helix and the axis of the β-sheet. This angle is 50° in MTX, whereas it is close to 25° in [A_{12},A_{20}]MTX.

Such a decrease in the angle between the axis of the α-helix and the axis of the β-sheet has also been observed in a three-disulfide-bridged MTX analog, [Abu_{19}, Abu_{34}]MTX, which was designed to restore the consensus motif of scorpion toxins [12]. In this analog, which possesses half-cystine pairings of the type C1-C4, C2-C5 and C3-C6, the angle is of 0°. This change in angle was correlated with modifications in pharmacology. Therefore, we studied the pharmacological activity of [A_{12},A_{20}]MTX onto apamin-sensitive SK and a number of voltage-gated Kv channels. We first tested the ability of [A_{12},A_{20}]MTX to compete with [^{125}I]apamin for binding onto rat brain synaptosomes. Fig. 4 shows an [A_{12},A_{20}]MTX-induced, concentration-dependent, inhibition of [^{125}I]apamin binding with a IC_{50} of 310 ± 100 nM. In comparison, synthetic MTX and unlabeled apamin completely inhibited [^{125}I]apamin binding with IC_{50}'s of 11 ± 10 nM and 0.52 ± 0.11 pM. This indicates that the proline substitutions in MTX result in a 30-fold decrease in binding affinity of the peptide for SK type channels. This can be compared with the 9-fold reduction in affinity observed for [Abu_{19}, Abu_{34}]MTX. Next, we determined the inhibitory effect of [A_{12},A_{20}]MTX on K^+ currents that result from the expression of *Shaker* B, rat Kv1.2 and Kv1.3 in *Xenopus* oocytes. Fig. 5A illustrates a representative inhibition of *Shaker* B currents by 500 nM [A_{12},A_{20}]MTX. The extent of inhibition was identical for various membrane depolarization values demonstrating the lack of strong voltage dependence in the peptide action. Dose-response experiments demonstrate that [A_{12},A_{20}]MTX inhibits up to 94% *Shaker* B currents with an IC_{50} of 130 ± 123 nM (n = 18; Fig. 5B). A similar maximal inhibition (92%) has also been observed for sMTX, albeit with an IC_{50} of 2.5 nM which corresponds to a 52-fold higher affinity than that observed with [A_{12},A_{20}]MTX for *Shaker* B channels [13]. We also tested the effect of singly substituted analogs of MTX on *Shaker* currents and observed IC_{50}'s of 1.1 ± 0.7 nM for [A_{12}]MTX (n = 24) and 1.4 ± 1.4 nM for [A_{20}]MTX (n = 26) (data not shown). These values are thus similar to sMTX and suggest that in the case of *Shaker* channel, disulfide bridge rearrangement of MTX does not affect blocking properties. In the case of the [A_{12},A_{20}]MTX analog, there are probably some greater alterations in toxin structure which may be responsible for its decreased potency in blocking *Shaker* channels. As for sMTX, the [A_{12},A_{20}]MTX analog had no effect on rat Kv1.1 (data not shown). It retained a significant activity onto rat Kv1.2 channels, as it inhibits 59 ± 23% of the K^+ currents with an IC_{50} of 0.68 ± 0.06 nM (n = 12). This affinity of [A_{12},A_{20}]MTX for Kv1.2 is about 10-fold lower than the IC_{50} of 0.06 nM reported for sMTX [12]. We were unable to measure a precise binding affinity of [A_{12},A_{20}]MTX for rat Kv1.3 although it appeared to block the current to a small extent (less than

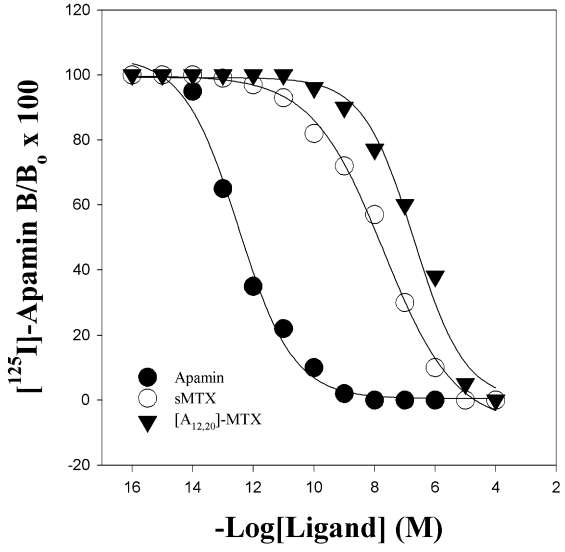

Fig. 4. Inhibition of [^{125}I]apamin binding onto rat brain synaptosomes by unlabeled apamin, sMTX and [A_{12},A_{20}]MTX. Dose-dependent inhibitions of [^{125}I]apamin binding are fitted by the equation $y = a/[1+\exp(-(x-IC_{50})/b)]$ with IC_{50} values of 310 ± 100 nM ([A_{12},A_{20}]MTX), 11 ± 10 nM (sMTX) and 0.52 ± 0.11 pM (unlabeled apamin). B_0 is the binding of [^{125}I]apamin in the absence of ligand, and B is the binding in the presence of the indicated concentration of competitors. Non-specific binding, less than 10%, was subtracted for the calculation of the ratios.

20%, $n = 8$) at high micromolar concentrations. A gross estimate of binding affinities suggests that there is also a 10-fold decrease in affinity induced by the proline substitutions.

Several novel information emerge from this study. First, it appears that the two proline residues in positions 12 and 20 play a pivotal role at least with regard to the disulfide bridge organization of MTX. Substitutions of these imino acid residues by alanyl induce a shift from the MTX half-cystine pairings (C1–C5, C2–C6, C3–C4 and C7–C8) towards a Pi1/HsTx1 disulfide bridge pattern (C1–C5, C2–C6, C3–C7 and C4–C8). The intimate molecular mechanism(s) underlying these changes in disulfide bridging have not yet been elucidated; however, one can envision that the two proline residues strongly favor the formation of the 'non-conventional' C3–C4 pairing in natural MTX, and that selective point mutations of these residues result in removal of such key prolyl-associated structural constraints. In turn, this change would favor a structural organization of the toxin towards a more 'conventional' disulfide bridge arrangement. Second, it is noteworthy that disulfide bridge reorganization in MTX results in a repositioning of the axis of the α-helix with regard to that of the β-sheet. Such a repositioning was not only observed in [A_{12},A_{20}]MTX (shift from an angle of 50° to 25°), but also in [Abu_{19},Abu_{34}]MTX (shift from an angle of 50° to 0°). These results are to be opposed to the observation that the fourth disulfide bridge in HsTx1 contributes little to the structure of HsTx1 [14]. Of interest for MTX, the relative orientation of the α-helix with regard to the main axis of the β-sheet measured on all available scorpion toxins from the Protein Data Bank files ranges from 0° to 70°, making this feature amino acid sequence-dependent. Our data strongly reinforce such an hypothesis. In addition, these data point out that the relative positions of half-cystine residues within the whole sequence are not the sole determinant guiding the disulfide bridge framework and α-helix positioning. This rearrangement in disulfide bridges, accompanied by a reorienta-

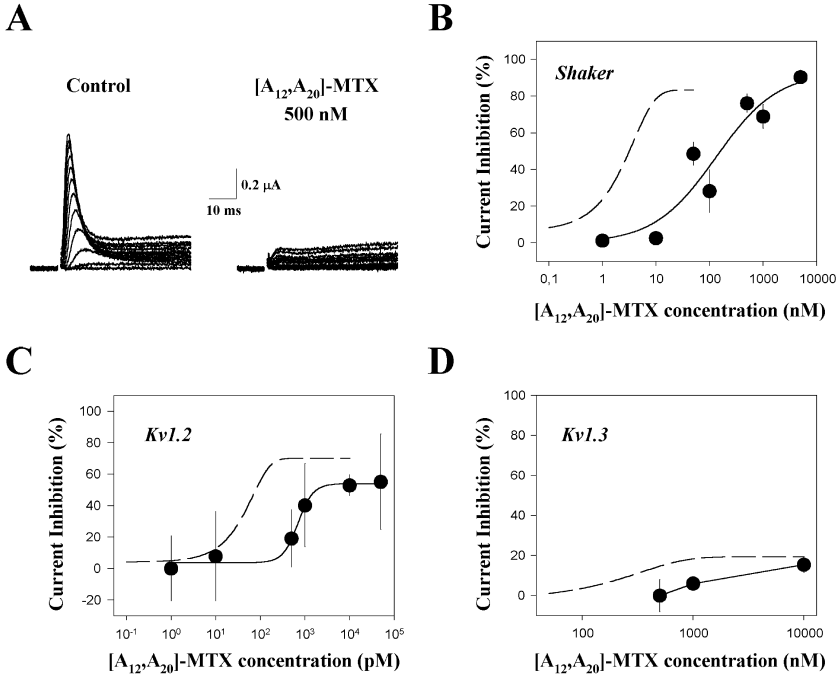

Fig. 5. [A_{12},A_{20}]MTX is a Kv type K^+ channel blocker. A: Oocyte expressing *Shaker* B K^+ currents recorded under two-electrode voltage clamp. Currents were obtained by depolarization from −90 mV to various potentials (from −40 to 70 mV by 10 mV increments). Left: control currents. Right: currents during superfusion of 500 nM [A_{12},A_{20}]MTX, illustrating over 80% block. B–D: Dose-dependent inhibition curves of *Shaker* B, rat Kv1.2 and rat Kv1.3 currents by [A_{12},A_{20}]MTX (filled circles). Dashed lines represent dose-dependent inhibition curves for sMTX and are shown for comparison. Data points at the mean ± S.E.M. The solid lines for the data are from the equation $y = a/[1+\exp(-(x-IC_{50})/b)]$ with IC_{50} values of 130 ± 123 nM (*Shaker* B, $n = 18$) and 0.68 ± 0.06 nM (rat Kv1.2, $n = 12$).

tion of the α-helix, could be, in each case, linked to changes in pharmacological sensitivity, suggesting that 3D repositioning of key amino acid residues critical to K^+ current blockage is likely to occur. The change in angle value between the α-helix and the β-sheet is unlikely to fully support the variation in peptide pharmacology towards Kv1.3. In [$Abu_{19,34}$]MTX, with an angle value of 0°, we noticed an enhancement of current blockade [12]. In contrast, a reduction in blockade potency was observed for [A_{12},A_{20}]MTX in spite of a similar reduction in the angle between the two secondary structures. Whatever the observed changes, these observations are all consistent with the assumption that the integrity of the MTX C-terminus is pivotal to Kv1.3 pharmacology [15].

Acknowledgements: We wish to thank S. Canarelli for helpful assistance. Z.F. is a recipient of a fellowship from Cellpep S.A. and the region Provence-Alpes-Côte d'Azur.

References

[1] Kharrat, R., Mabrouk, K., Crest, M., Darbon, H., Oughideni, R., Martin-Eauclaire, M.F., Jacquet, G., El Ayeb, M., Van Rietschoten, J., Rochat, H. and Sabatier, J.M. (1996) Eur. J. Biochem. 242, 491–498.
[2] Olamendi-Portugal, T., Gomez-Lagunas, F., Gurrola, G.B. and Possani, L.D. (1996) Biochem. J. 315, 977–981.
[3] Lebrun, B., Romi-Lebrun, R., Martin-Eauclaire, M.F., Yasuda, A., Ishiguro, M., Oyama, Y., Pongs, O. and Nakajima, T. (1997) Biochem. J. 328, 321–327.
[4] Fajloun, Z., Carlier, E., Lecomte, C., Geib, S., di Luccio, E., Bichet, D., Mabrouk, K., Rochat, H., De Waard, M. and Sabatier, J.M. (2001) Eur. J. Biochem., submitted for publication.
[5] Merrifield, R.B. (1986) Science 232, 341–347.
[6] Gray, E.G. and Whittaker, V.P. (1962) J. Anat. 96, 79–88.
[7] Seagar, M., Granier, C. and Couraud, F. (1984) J. Biol. Chem. 259, 1491–1495.
[8] De Waard, M. and Campbell, K.P. (1995) J. Physiol. 485, 619–634.
[9] Eppig, J.J. and Dumont, J.N. (1976) In Vitro 12, 418–427.
[10] Delepierre, M., Prochnicka-Chalufour, A. and Possani, L.D. (1998) Toxicon 36, 1599–1608.
[11] Sabatier, J.M. (1999) in: Handbook of Toxinology, Animal Toxins: Tools in Cell Biology (Rochat, H. and Martin-Eauclaire, M.F., Eds.), pp. 198–218, Birkhäuser, Basel.
[12] Fajloun, Z., Ferrat, G., Carlier, E., Fathallah, M., Lecomte, C., Sandoz, G., di Luccio, E., Mabrouk, K., Legros, C., Darbon, H., Rochat, H., Sabatier, J.-M. and De Waard, M. (2000) J. Biol. Chem. 275, 13605–13612.
[13] Carlier, E., Avdonin, V., Geib, S., Fajloun, Z., Kharrat, R., Rochat, H., Sabatier, J.-M., Hoshi, T. and De Waard, M. (2000) J. Peptide Res. 55, 419–427.
[14] Savarin, P., Romi-Lebrun, R., Zinn-Justin, S., Lebrun, B., Nakajima, T., Gilquin, B. and Ménez, A. (1999) Protein Sci. 8, 2672–2685.
[15] Lecomte, C., Ben Khalifa, R., Martin-Eauclaire, M.F., Kharrat, R., El Ayeb, M., Darbon, H., Rochat, H., Crest, M. and Sabatier, J.M. (2000) J. Peptide Res. 55, 246–254.